# 3-D Unitary ESPRIT for Joint 2-D Angle and Carrier Estimation

*Martin Haardt*
Siemens AG, ÖN MN P 36
Hofmannstr. 51
D-81359 Munich, Germany

*Josef A. Nossek*
Inst. of Network Theory & Circuit Design
Technical University of Munich
D-80290 Munich, Germany

*Abstract* — **It is essential for an efficient frequency and time slot allocation procedure in future mobile communication systems using space division multiple access (SDMA) to determine the mobiles that are spatially well separated from one another. Thus, once a mobile desires to initiate a call, precise knowledge of the 2-D arrival angles of its dominant wavefronts is required. In this application, 3-D Unitary ESPRIT for joint 2-D angle and carrier estimation offers an efficient way to handle such mobile access requests since it provides efficient high-resolution measurements of the spatial characteristics of the wireless channel, even if only a small number of antennas is available at the base station. Automatic pairing of the 3-D estimates is achieved via a new simultaneous Schur decomposition (SSD) of three real-valued, non-symmetric matrices. In general, the SSD enables an $R$-dimensional extension of Unitary ESPRIT ($R \geq 3$) to estimate several undamped $R$-dimensional modes or frequencies along with their correct pairing in multidimensional harmonic retrieval problems. Here, we present a Jacobi-type method to calculate the SSD. For each of the $R$ dimensions, the corresponding frequency estimates are obtained from the real eigenvalues of a real-valued matrix. The SSD jointly estimates the eigenvalues of all $R$-matrices and, thereby, achieves automatic pairing of the estimated $R$-dimensional modes via a closed-form procedure that neither requires any search nor any other heuristic pairing strategy.**

## 1. Introduction

Due to its simplicity and high-resolution capability, *ESPRIT* has become one of the most popular subspace-based direction of arrival or frequency estimation schemes. For certain array geometries, namely centro-symmetric arrays, or undamped modes the computational complexity can be reduced significantly by formulating an ESPRIT-type algorithm in terms of real-valued computations throughout. The resulting algorithm is called *Unitary ESPRIT* since the estimated phase factors are automatically constrained to the unit circle [5]. Furthermore, *Unitary ESPRIT* has recently been extended to the 2-D case to provide automatically paired azimuth and elevation angle estimates [6, 11, 3]. If, however, the carrier frequencies of the impinging wavefronts are no longer known (e.g., due to Doppler shifts) and may differ, the 2-D arrival angles, azimuth and elevation, and the corresponding carrier frequencies have to be estimated simultaneously. This model applies, for instance, to the surveillance radar system discussed in [10] and requires a 3-D extension of Unitary ESPRIT.

This research was performed while M. Haardt was with the Institute of Network Theory and Circuit Design, Technical University of Munich, D-80290 Munich, Germany. It was supported by the German Research Foundation (DFG) under contract number 322-730. The authors would like to thank Prof. Werner Wiesbeck and his research group (University of Karlsruhe, Germany) for providing the results of their 3-D ray tracing simulations. Their help is gratefully acknowledged.

## 2. Mobile Access Requests in SDMA Applications

In future mobile communication systems, space division multiple access (SDMA) will enable mobiles that are located at spatially distinct angles from the base station to operate on the same frequency as well as in the same time slot [9]. Therefore, it is essential for an SDMA frequency and time slot allocation procedure to determine the mobiles that are *spatially well separated* from one another. Thus, once a mobile desires to initiate a call, precise knowledge of the 2-D arrival angles of its dominant wavefronts is required. These estimated 2-D arrival angles can also be used for efficient downlink beamforming.

3-D Unitary ESPRIT for joint 2-D angle and carrier estimation offers an efficient way to handle such mobile access requests in mobile communication systems using SDMA, since it provides efficient high-resolution measurements of the spatial characteristics of the wireless channel. In this application, all users in a particular

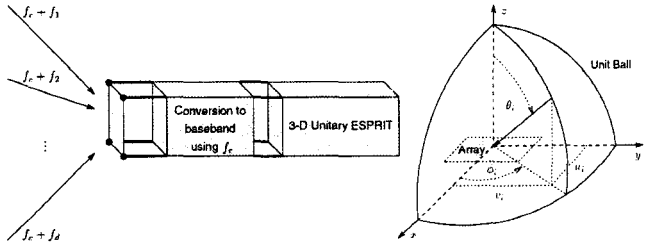


**Figure 1:** Using noise-corrupted measurements from an antenna array at the base station, 3-D Unitary ESPRIT estimates the 2-D arrival angles, frequency offsets, and attenuation factors of the dominant multipaths of all users that transmit on the access request channel, as illustrated on the left side. Azimuth ($-180° < \phi_i \leq 180°$), elevation ($0° \leq \theta_i \leq 90°$), and the direction cosines $u_i$ and $v_i$ are defined on the right side of this figure.

cell are assigned individual pilot tones that are transmitted on a separate *access request channel* if a user wants to initiate a call. The frequencies of these pilot tones can be quite close to one another. It is a major advantage of the proposed technique that neither synchronization nor carrier recovery is required on the access request channel. Using noise-corrupted measurements from an antenna array at the base station,[1] 3-D Unitary ESPRIT jointly estimates the *2-D arrival angles* and *frequencies* of the dominant multipath components, cf. Figure 1. Notice that the precise carrier frequencies of the dominant multipaths are usually unknown since the oscillators at the transmitters have certain tolerances. Moreover, the estimated frequencies enable us to assign the corresponding 2-D arrival angles to the different users that transmit on the access request channel. After estimating the 2-D arrival angles and the associated carrier

[1] As in the 2-D case, the antenna array must be centro-symmetric and exhibit a dual invariance structure [6, 3].

0-8186-7919-0/97 $10.00 

frequencies, the *attenuation factors* of these dominant multipaths can be obtained via a simple least squares fit.

Let the frequencies $(f_c + f_i)$, $1 \le i \le d$, be the precise carrier frequencies of the $d$ dominant multipath components, where $f_c$ denotes an approximate "center" frequency of the assigned (nominal) pilot tones. Then, the noise-corrupted measurements are converted to "baseband" using the carrier $f_c$ as illustrated on the left side of Figure 1. Afterwards, 3-D Unitary ESPRIT operates on these down-converted measurements and jointly estimates the three components of the frequency vectors $\boldsymbol{\mu}_i = [\ \mu_i^{(1)} \quad \mu_i^{(2)} \quad \mu_i^{(3)}\ ]$ with

$$\mu_i^{(1)} = \frac{2\pi(f_c + f_i)}{c}\Delta_x u_i, \quad \mu_i^{(2)} = \frac{2\pi(f_c + f_i)}{c}\Delta_y v_i,$$

$$\text{and} \quad \mu_i^{(3)} = 2\pi f_i T_s, \quad 1 \le i \le d,$$

for all dominant multipath components. Here, $u_i = \cos\phi_i \sin\theta_i$ and $v_i = \sin\phi_i \sin\theta_i$, $1 \le i \le d$, are the direction cosines of the $i$th source relative to the $x$- and $y$-axes as illustrated on the right side of Figure 1. Moreover, $c$ denotes the propagation velocity, $\Delta_x$ and $\Delta_y$ the sensor distances in $x$- and $y$-direction, and $T_s$ the sampling interval.

## 3. Multidimensional Extension of Unitary ESPRIT

In the more general $R$-dimensional case, the $d$ frequency vectors

$$\boldsymbol{\mu}_i = [\ \mu_i^{(1)} \quad \mu_i^{(2)} \quad \dots \quad \mu_i^{(R)}\ ], \quad 1 \le i \le d, \qquad (1)$$

that correspond to the $d$ $R$-dimensional modes, and their correct pairing are estimated from the noise-corrupted measurements [4, 3].

A very simple and efficient way to achieve this goal would be an $R$-dimensional extension of *Unitary ESPRIT* [4, 3]. As in the 1-D case [5], the algorithm is formulated in terms of real-valued computations throughout. After the computation of a basis for the estimated signal subspace through a real-valued SVD of the transformed data matrix, $R$ overdetermined real-valued systems of equations can be formed. They are solved independently via least squares, total least squares, or structured least squares [3] yielding $R$ real-valued matrices $\boldsymbol{\Upsilon}_r \in \mathbb{R}^{d\times d}$, $1 \le r \le R$. Note that these matrices are not necessarily symmetric.

In the noiseless case or with an infinite number of experiments $N$, the $R$ least squares solutions $\boldsymbol{\Upsilon}_r$ admit the following eigendecompositions

$$\boldsymbol{\Upsilon}_r = \boldsymbol{T}\,\boldsymbol{\Omega}_r\boldsymbol{T}^{-1} \quad \text{with} \quad \boldsymbol{\Omega}_r = \operatorname{diag}\left\{\tan\left(\frac{\mu_i^{(r)}}{2}\right)\right\}_{i=1}^{d}, \qquad (2)$$

$1 \le r \le R$. Notice first that all the matrices in (2) are real-valued. Secondly, if the matrix of eigenvectors $\boldsymbol{T} \in \mathbb{R}^{d\times d}$ in the spectral decomposition of $\boldsymbol{\Upsilon}_r = \boldsymbol{T}\,\boldsymbol{\Omega}_r\boldsymbol{T}^{-1}$ is the same for all $r$, $1 \le r \le R$, the diagonal elements of the matrices $\boldsymbol{\Omega}_r$ and, therefore, also the desired frequencies in (1) are automatically paired.

In practice, though, only a finite number $N$ of noise-corrupted experiments (or measurements) is available. Therefore, the $R$ matrices $\boldsymbol{\Upsilon}_r$ do not exactly share the same set of eigenvectors. To determine the set of eigenvectors only from one of the $\boldsymbol{\Upsilon}_r$ is, obviously, not the best solution, since this strategy would rely on an arbitrary choice and would also discard information contained in the other $R-1$ matrices. Moreover, each of the $\boldsymbol{\Upsilon}_r$ might have some degenerate (multiple) eigenvalues, while the whole set $\boldsymbol{\Upsilon}_r$, $1 \le r \le R$, has well determined common eigenvectors $\boldsymbol{T}$ (for $N \to \infty$ or $\sigma_N^2 \to 0$). Thus, from a statistical point of view and for the sake of accuracy and robustness, it is desirable to compute the "average eigenstructure" of these matrices [2]. In the 2-D case, automatic pairing can be achieved by calculating the eigenvalues of the "complexified" matrix $\boldsymbol{\Upsilon}_1 + \mathrm{j}\boldsymbol{\Upsilon}_2 \in \mathbb{C}^{d\times d}$, cf. the derivation of 2-D Unitary ESPRIT in [6, 11, 3]. If, however, $R > 2$, this "trick" has to be extended to the $R$-dimensional case. To this end, we will present a Jacobi-type method to calculate a simultaneous Schur decomposition (SSD) of several matrices.

## 4. Simultaneous Schur Decomposition (SSD)

Recall that the real eigenvalues of a real-valued non-symmetric matrix can efficiently be computed through an eigenvalue-revealing real Schur decomposition. In the noiseless case or with an infinite number of experiments $N$, the new SSD of the $R$ matrices $\boldsymbol{\Upsilon}_r$, $1 \le r \le R$, yields $R$ (real-valued) upper triangular matrices that exhibit the automatically paired eigenvalues on their main diagonals. Under the assumption of additive noise and a finite number of experiments $N$, an orthogonal similarity transformation might not be able to produce $R$ upper triangular matrices simultaneously, since the $R$ "noisy" matrices do not share a common set of eigenvectors. In this case, the resulting matrices should be "almost" upper triangular in a least squares sense as explained in the sequel.

To derive an appropriate algorithm, let $\mathcal{L}(\boldsymbol{\Upsilon}_r)$ denote an operator that extracts the strictly lower triangular part of its matrix-valued argument by setting the upper triangular part and the elements on the main diagonal to zero. Then, we want to minimize the cost function

$$\psi(\boldsymbol{\Theta}) = \sum_{r=1}^{R} \left\| \mathcal{L}(\boldsymbol{\Theta}^T \boldsymbol{\Upsilon}_r \boldsymbol{\Theta}) \right\|_{\mathrm{F}}^2 \qquad (3)$$

over the set of orthogonal matrices $\boldsymbol{\Theta} \in \mathbb{R}^{d\times d}$ that can be written as products of elementary Jacobi rotations. As usual, $\|\cdot\|_{\mathrm{F}}$ denotes the Frobenius norm.[2]

In Jacobi-type algorithms, the orthogonal matrix $\boldsymbol{\Theta}$ is decomposed into a product of elementary Jacobi rotations

$$\boldsymbol{\Theta}_{qp} = \begin{bmatrix} 1 & \cdots & 0 & \cdots & 0 & \cdots & 0 \\ \vdots & & \vdots & & \vdots & & \vdots \\ 0 & \cdots & c & \cdots & s & \cdots & 0 \\ \vdots & & \vdots & & \vdots & & \vdots \\ 0 & \cdots & -s & \cdots & c & \cdots & 0 \\ \vdots & & \vdots & & \vdots & & \vdots \\ 0 & \cdots & 0 & \cdots & 0 & \cdots & 1 \end{bmatrix} \qquad (4)$$

such that

$$\boldsymbol{\Theta} = \prod_{\#\text{ of sweeps}} \prod_{q=1}^{d} \prod_{p=1}^{q-1} \boldsymbol{\Theta}_{qp}. \qquad (5)$$

Jacobi rotations $\boldsymbol{\Theta}_{qp}$ are defined such that all diagonal elements of $\boldsymbol{\Theta}_{qp}$ are 1 except for the two elements $c$ in rows (and columns) $p$ and $q$. Likewise, all off-diagonal elements of $\boldsymbol{\Theta}_{qp}$ are 0 except for the two elements $s$ and $-s$, cf. (4). The real numbers $c = \cos\vartheta$ and $s = \sin\vartheta$ are the cosine and sine of a rotation angle $\vartheta$. In the sequel, we describe a procedure to choose the rotation angle $\vartheta$ at a particular iteration such that the cost function $\psi(\boldsymbol{\Theta})$ is decreased as

[2] If all the $\boldsymbol{\Upsilon}_r$ were symmetric, the minimization of (3) would achieve an approximate simultaneous *diagonalization* of these matrices. An efficient Jacobi-type technique to achieve such an approximate simultaneous diagonalization has been presented in [1, 2]. This algorithm, however, is not applicable in our case, since the $\boldsymbol{\Upsilon}_r$ are not symmetric. Therefore, the minimization of the sum of the off-diagonal norms of these $R$ matrices via a sequence of simultaneous orthogonal transformations as discussed in [1, 2] would not reveal the desired "average eigenstructure" of these non-symmetric matrices.

much as possible. To this end, observe that, at each iteration, the $R$ real-valued matrices $\boldsymbol{\Upsilon}_r$ are transformed according to

$$\boldsymbol{\Upsilon}'_r = \boldsymbol{\Theta}_{qp}^T \boldsymbol{\Upsilon}_r \boldsymbol{\Theta}_{qp}, \quad 1 \le r \le R. \tag{6}$$

It is easily seen that the orthogonal transformation (6) changes only elements of $\boldsymbol{\Upsilon}_r$ that appear in rows and columns $p$ and $q$. The change of the cost function (3) at this iteration may be expressed as

$$\Delta\psi\left(\boldsymbol{\Theta}_{qp}\right) = \sum_{r=1}^{R} \left( \left\| \mathcal{L}(\boldsymbol{\Upsilon}'_r) \right\|_{\mathrm{F}}^2 - \left\| \mathcal{L}(\boldsymbol{\Upsilon}_r) \right\|_{\mathrm{F}}^2 \right). \tag{7}$$

Let $v_{k\ell}^{(r)}$ denote the $(k,\ell)$-entries of the matrices $\boldsymbol{\Upsilon}_r$, $1 \le r \le R$. In [4], it was shown that the critical points of $\Delta\psi\left(\boldsymbol{\Theta}_{qp}\right)$ in (7) can be obtained from the real-valued roots of the fourth order polynomial

$$p(t) = \begin{bmatrix} 1 & t & t^2 & t^3 & t^4 \end{bmatrix} \cdot \sum_{r=1}^{R} \boldsymbol{c}^{(r)}. \tag{8}$$

Its real-valued coefficients are easily constructed from the entries of the $R$ matrices $\boldsymbol{\Upsilon}_r$, namely

$$\boldsymbol{c}^{(r)} = \boldsymbol{c}_{qp}^{(r)} + \sum_{k=(p+1)}^{q-1} \left( \boldsymbol{c}_{\mathrm{add}}(v_{pk}^{(r)}, v_{qk}^{(r)}) - \boldsymbol{c}_{\mathrm{add}}(v_{kp}^{(r)}, v_{kq}^{(r)}) \right),$$

$$\boldsymbol{c}_{qp}^{(r)} = \begin{bmatrix} v_{qp}^{(r)} \cdot (v_{pp}^{(r)} - v_{qq}^{(r)}) \\ (v_{pp}^{(r)} - v_{qq}^{(r)})^2 - 2v_{qp}^{(r)} \cdot (v_{pq}^{(r)} + v_{qp}^{(r)}) \\ -3 \cdot (v_{pp}^{(r)} - v_{qq}^{(r)}) \cdot (v_{pq}^{(r)} + v_{qp}^{(r)}) \\ -(v_{pp}^{(r)} - v_{qq}^{(r)})^2 + 2v_{pq}^{(r)} \cdot (v_{pq}^{(r)} + v_{qp}^{(r)}) \\ v_{pq}^{(r)} \cdot (v_{pp}^{(r)} - v_{qq}^{(r)}) \end{bmatrix},$$

and $\boldsymbol{c}_{\mathrm{add}}(a,b) = \begin{bmatrix} a \cdot b & a^2 - b^2 & 0 & a^2 - b^2 & -a \cdot b \end{bmatrix}^T$.

Observe that only the real-valued roots of $p(t)$ yield valid options for the desired orthogonal rotation $\boldsymbol{\Theta}_{qp}$. A real-valued critical point of $\Delta\psi\left(\boldsymbol{\Theta}_{qp}\right)$ is a minimum if

$$\frac{d}{d\vartheta} \left( \frac{p(\tan\vartheta)}{(1+\tan^2\vartheta)^2} \right) > 0.$$

Straightforward calculations show that this condition is met if

$$\frac{dp(t)}{dt} = c_1 + 2c_2 t + 3c_3 t^2 + 4c_4 t^3 > 0, \tag{9}$$

$$\text{where} \quad \begin{bmatrix} c_0 & c_1 & c_2 & c_3 & c_4 \end{bmatrix}^T = \sum_{r=1}^{R} \boldsymbol{c}^{(r)}$$

and $t = \tan\vartheta$. Notice that there are at most two real-valued roots that satisfy (9). From these possibilities, we choose the value of $t$ (or the corresponding rotation angle $\vartheta$) that minimizes (7). However, we only use the corresponding elementary Jacobi rotation $\boldsymbol{\Theta}_{qp}$ if

$$\Delta\psi\left(\boldsymbol{\Theta}_{qp}\right) < 0,$$

i.e., the chosen rotation reduces the cost function. Otherwise, no rotation is applied at this particular iteration step. Such a strategy is closely related to the one-dimensional Jacobi-type methods discussed in [7].

If $c_4$, the coefficient of $t^4$ in (8), i.e., the last component of the coefficient vector $\sum_{r=1}^{R} \boldsymbol{c}^{(r)}$, equals zero, $p(t)$ reduces to a third order polynomial. Then $t = \infty$ is also a critical point of $\Delta\psi\left(\boldsymbol{\Theta}_{qp}\right)$. It corresponds to a valid option for the rotation angle $\vartheta$, i.e., a minimum of $\Delta\psi\left(\boldsymbol{\Theta}_{qp}\right)$, if $c_3 > 0$.

**Table 1:** Simulation parameters obtained from 3-D ray tracing. The corresponding map locations of the base station and the mobile users can be identified in Figure 2. Moreover, the number of individual wavefronts and the frequencies $f_i$ are listed ($f_c = 1000$ MHz).

| user | map location | # of simulated wavefronts | $f_i$ |
|---|---|---|---|
| 1 | 306 | 278 | -20 kHz |
| 2 | 360 | 83 | -15 kHz |
| 3 | 406 | 319 | -10 kHz |
| 4 | 420 | 77 | -5 kHz |
| 5 | 600 | 335 | 0 kHz |
| 6 | 720 | 146 | 5 kHz |
| 7 | 980 | 747 | 10 kHz |
| 8 | 1013 | 127 | 15 kHz |

## 5. Simulations Based on Ray Tracing Using a Topographical Map of Munich

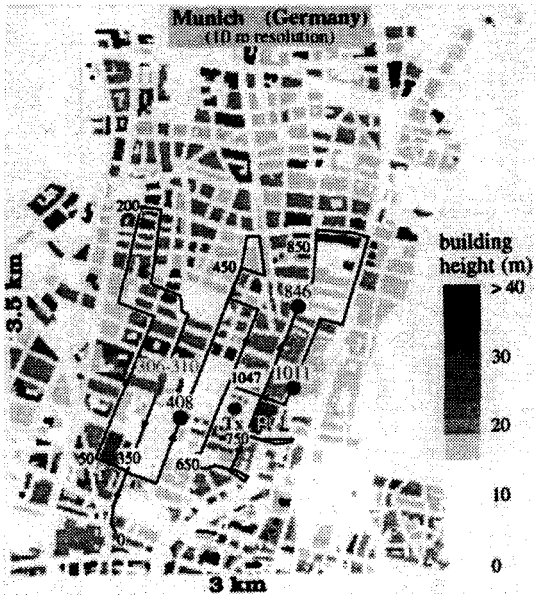


**Figure 2:** Rastered map of downtown Munich showing the location of the base station (Tx) and a route containing 1050 measurement points.

The presented simulation results use realistic 2-D arrival angles derived from a ray tracing program for macrocell environments [8]. They are based on a three-dimensional topographical model of downtown Munich, where the height of the base station was 26 meters and the height of the transmitter at the mobiles 2 meters. The heights of most buildings varied between 10 and 30 meters as depicted in Figure 2. In this urban environment, the propagation conditions at $f_c = 1000$ MHz were predicted via 3-D ray tracing, taking into account wave interactions like diffraction and scattering over each propagation path [8]. Ray tracing tools developed at the University of Karlsruhe provided the channel impulse response of each propagation path in terms of its attenuation, time delay, 2-D launching angle (at the transmitter), and 2-D arrival angle (at the receiver). The resulting coverage predictions agree with measurements taken in the same urban area.

In the simulations, we have used 8 users, and a random phase shift was assigned to each propagation path. Furthermore, we have employed a uniform rectangular array (URA) of $M_1 \times M_2 = 4 \times 4$ antennas and a window length of $M_3 = 625$ snapshots. The geographical locations of the 8 mobile users in downtown Munich and the geographical location of the base station (Tx) are depicted in Figure 2. Notice that the corresponding map locations and carrier frequencies $f_c + f_i$ of the mobile users are specified in Table 1. The number of simulated wavefronts per mobile user is also listed

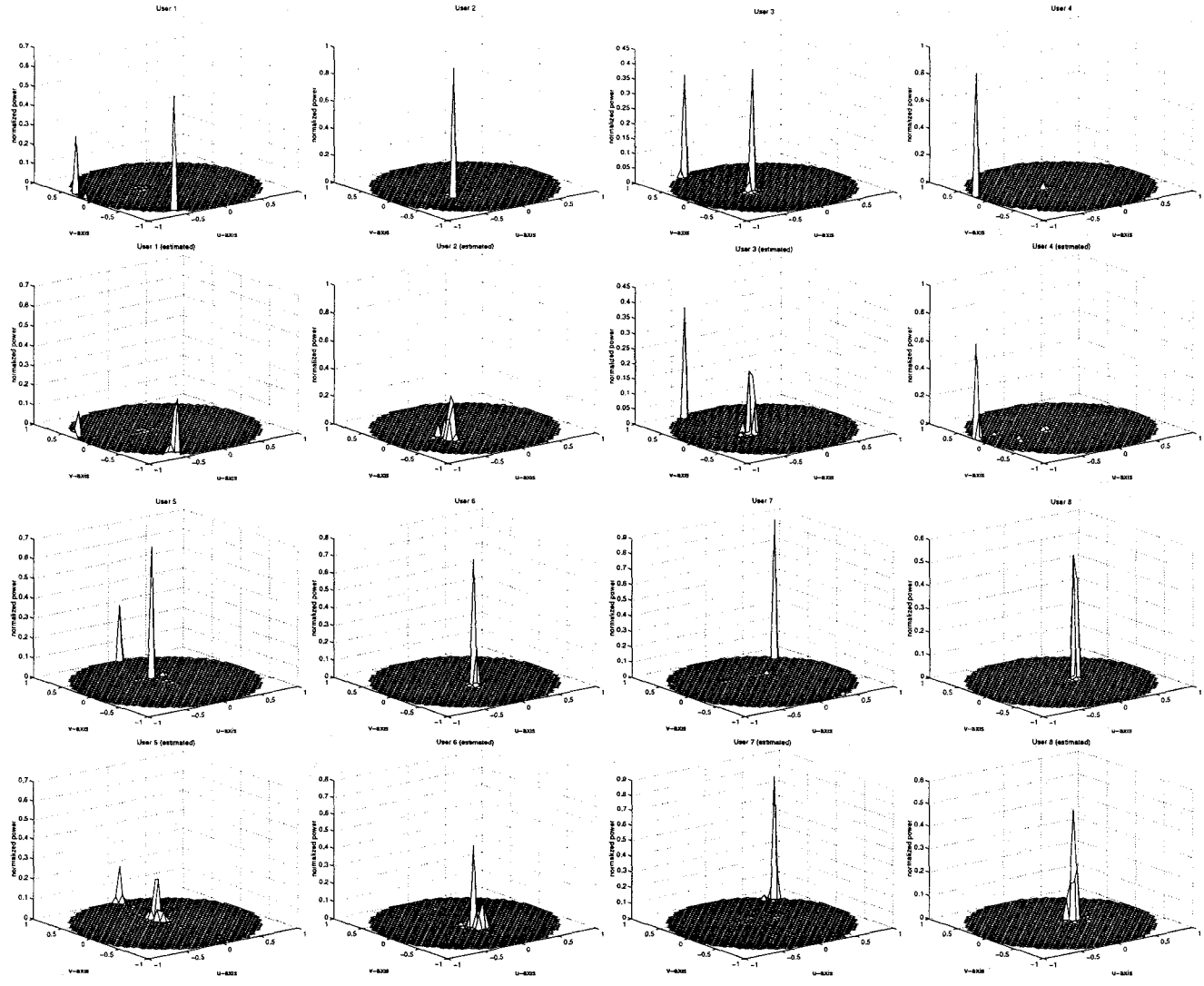

**Figure 3:** Simulation results obtained with 3-D Unitary ESPRIT and a URA of $M_1 \times M_2 = 4 \times 4$ elements, $M_3 = 625$ snapshots, and a sampling interval of $T_s = 7.385$ $\mu$s (smoothing parameters: $L_1 = 1, L_2 = 2, L_3 = 501$). The figures on the top (1st and 3rd row) show the 2-D arrival angles for the 8 users of Table 1, predicted via ray tracing, and their associated power as a function of the direction cosines in the $u$-$v$ plane, while the figures on the bottom (2nd and 4th row) depict the estimated power in the $u$-$v$ plane, averaged over 20 trials. Clearly, the dominant 2-D arrival angles of all users are identified correctly.

in Table 1. Rows 1 and 3 of Figure 3 illustrate the corresponding 2-D arrival angles at the base station predicted via 3-D ray tracing. More precisely, they show the power of the impinging wavefronts as a function of the direction cosines in the $u$-$v$ plane (linear scale). The power of the additive noise was 20 dB below the total power of each user.

To estimate the dominant 2-D arrival angles and the associated carrier frequencies, *3-D Unitary ESPRIT and LS* were used in conjunction with 3-D smoothing [3]. Rows 2 and 4 of Figure 3 depict the estimated 2-D arrival angles and their associated power, averaged over 20 trials. The estimated carrier frequencies were used to associate the estimated 2-D arrival angles with the 8 users. Although up to 747 individual wavefronts were simulated for each user, cf. Table 1, the dominant 2-D arrival angles of all 8 users are identified correctly.

## References


[1] J. F. Cardoso and A. Souloumiac, "Blind beamforming for non Gaussian signals", *IEE Proc.-F*, vol. 140, no. 6, pp. 362–370, Dec. 1993.

[2] J. F. Cardoso and A. Souloumiac, "Jacobi angles for simultaneous diagonalization", *SIAM J. Matrix Anal. Appl.*, vol. 17, pp. 161–164, Jan. 1996.

[3] M. Haardt, *Efficient One-, Two-, and Multidimensional High-Resolution Array Signal Processing*, Ph. D. dissertation, Technical University of Munich, Munich, Germany, 1996.

[4] M. Haardt, K. Hüper, J. B. Moore, and J. A. Nossek, "Simultaneous Schur decomposition of several matrices to achieve automatic pairing in multidimensional harmonic retrieval problems", in *Signal Processing VIII: Theories and Applications (Proc. of EUSIPCO-96)*, G. Ramponi, G. L. Sicuranza, S. Carrato, and S. Marsi, Eds., vol. I, pp. 531–534, Trieste, Italy, Sept. 1996, Edizioni LINT Trieste.

[5] M. Haardt and J. A. Nossek, "Unitary ESPRIT: How to obtain increased estimation accuracy with a reduced computational burden", *IEEE Trans. Signal Processing*, vol. 43, pp. 1232–1242, May 1995.

[6] M. Haardt, M. D. Zoltowski, C. P. Mathews, and J. A. Nossek, "2D Unitary ESPRIT for efficient 2D parameter estimation", in *Proc. IEEE Int. Conf. Acoust., Speech, Signal Processing*, vol. 3, pp. 2096–2099, Detroit, MI, May 1995.

[7] K. Hüper and U. Helmke, "Structure and convergence of Jacobi-type methods", Tech. Rep. TUM-LNS-TR-95-2, Technical University of Munich, Institute of Network Theory and Circuit Design, July 1995, submitted to *Numerische Mathematik*.

[8] T. Kürner, D. C. Cichon, and W. Wiesbeck, "Concepts and results for 3D digital terrain-based wave propagation models: An overview", *IEEE J. Select. Areas Commun.*, vol. 11, pp. 1002–1012, Sept. 1993.

[9] R. Rheinschmitt and M. Tangemann, "Performance of sectorised spatial multiplex systems", in *Proc. IEEE Vehicular Techn. Conf.*, vol. 1, pp. 426–430, Atlanta, GA, Apr. 1996.

[10] F. Vanpoucke, *Algorithms and Architectures for Adaptive Array Signal Processing*, Ph. D. dissertation, Katholieke Universiteit Leuven, Leuven, Belgium, Feb. 1995.

[11] M. D. Zoltowski, M. Haardt, and C. P. Mathews, "Closed-form 2D angle estimation with rectangular arrays in element space or beamspace via Unitary ESPRIT", *IEEE Trans. Signal Processing*, vol. 44, pp. 316–328, Feb. 1996.